Salinity dependence of spectral induced polarization in sands and sandstones

André Revil, Magnus Skold

Geophysical Journal International

Geophys. J. Int. (2011) **187,** 813–824 doi: 10.1111/j.1365-246X.2011.05181.x

Salinity dependence of spectral induced polarization in sands and sandstones

A. Revil[1,2] and M. Skold[1]

[1] *Colorado School of Mines, Department of Geophysics, Golden,* CO 80401, *USA. E-mail: arevil@mines.edu*
[2] *ISTerre, CNRS, UMR CNRS* 5275, *Université de Savoie,* 73376 *cedex, Le Bourget du Lac, France*

Accepted 2011 August 3. Received 2011 August 2; in original form 2011 February 27

SUMMARY

In electrolyte-saturated sands, the reversible storage of electrical charges is responsible for a phase lag between the current (injected and retrieved by two current electrodes) and the electrical field recorded by two voltage electrodes. This phenomenon is called 'spectral induced polarization' in geophysics and can potentially be used to monitor salt tracer tests in shallow aquifers to infer their permeability and dispersivity tensors. We demonstrate analytically that the polarization of the inner part of the electrical triple layer coating the surface of the grains (named the Stern layer in electrochemistry) is consistent with available data. We also perform new experiments using silica sands saturated by NaCl and $CaCl_2$ pore water solutions. The salinity dependence of quadrature conductivity can be modelled using an analytical solution of the triple layer model, which offers a simple way to interpret laboratory and field data. This analytical solution depends on the total site density of the mineral surface, the pH value and the sorption coefficient of the cation in the Stern layer. This model shows that both the specific surface conductivity of the Stern layer and the quadrature conductivity of the porous material depend on the conductivity of the pore water. The quadrature conductivity is becoming independent of the salinity above 1 S m^{-1}. The parameters entering the analytical model are consistent with independent estimates from titration data and zeta potential measurements, which are two classical methods to characterize the electrical triple layer at the pore water mineral interface.

Key words: Electrical properties; Electromagnetic theory; Hydrogeophysics; Permeability and porosity.

1 INTRODUCTION

The Spectral Induced Polarization (SIP) method is a geophysical method that has received a considerable attention in the recent literature. This method is used in biogeophysics to the detection of bacterial activity (Atekwana & Slater 2009; Williams *et al*. 2009). It is also used to characterize oil reservoirs and oil spills (Vinegar & Waxman 1984; Cassiani *et al*. 2009; Schmutz *et al*. 2010). In addition, because of its sensitivity to permeability (Börner 1992; de Lima & Niwas 2000; Slater & Lesmes 2002; Kemna *et al*. 2005; Revil & Florsch 2010), this method has been used to characterize the permeability distribution of shallow aquifers (Hördt *et al*. 2007). In SIP, a phase lag between the current and the electrical field provides complementary information to electrical conductivity measurements. The conductivity and the phase can be recasted into a complex conductivity (or a complex resistivity) that can be measured over a broad range of frequencies, typically from 1 mHz to few tens of kHz in the laboratory and from 10 mHz to 10–100 Hz in the field (Kemna 2000; Binley & Kemna 2005).

While DC ('direct current') resistivity tomography has been broadly used to characterize salt tracer tests in shallow aquifers, the SIP method has not. As a side note, the DC resistivity is always measured at some (low) frequency and the wording DC resistivity tomography is an approximation. Salt tracer tests monitored with DC resistivity have become increasingly popular in the recent literature for determining permeability and dispersivity of shallow aquifers (e.g. Pollock & Cirpka 2008; Müller *et al*. 2010 and references therein). However, DC resistivity monitoring has an intrinsic difficulty related to the existence of surface conductivity at the pore water mineral interface, which contributes to the effective conductivity of porous materials. Surface conductivity is related to electromigration of the charge carriers at the pore water mineral interface, in the so-called electrical triple layer coating the mineral water interface. Like the contribution associated with the bulk pore water (in the pore space), this contribution is salinity-dependent (Revil *et al*. 1999a). To avoid dealing with this problem, it is common among hydrogeologists and geophysicists working in field of hydrogeophysics to simply ignore this contribution (see, for instance, Singha & Gorelick 2005; Pollock & Cirpka 2008; Singha *et al*. 2008; see Müller *et al*. 2010 for an exception to this rule). Neglecting surface conductivity may result in overselling what can be accomplished with the interpretation of time-lapse DC

resistivity monitoring of salt tracer tests. Indeed, such an assumption can lead to spurious interpretations, as it is known that even in silica sands, surface conductivity cannot always be ignored at very low salinities (see Bolève *et al*. 2007 and Jardani *et al*. 2009 for some examples). There is however a remedy to this problem. Indeed, SIP offers an independent way to estimate surface conductivity (Revil & Florsch 2010), and especially changes in surface conductivity associated with changes in salinity. If the salinity dependence of SIP is well understood, it offers therefore a simple approach to monitor salt plume tracer avoiding the assumption of neglecting surface conductivity commonly made by hydrogeologists.

The problem with SIP is that it has been treated mostly on empirical grounds in the geophysical community because of the variety of competing polarization mechanisms existing in porous media. It is customary to fit SIP measurements with empirical models (e.g. Debye, Cole-Cole, and Cole Davidson, see Cole & Cole 1941, Cassiani *et al*. 2009 for instance). However, such an approach is not satisfactory because hydrogeologists and hydrogeochemists are not interested in the distribution of the Cole–Cole parameters. They are interested in the 3-D determination of permeability and dispersivity tensors. The problem with developing a quantitative interpretation of induced polarization data is associated with the existence of a variety of competing mechanisms. In an abiotic porous material with no metallic particles, there are five mechanisms that have been envisioned in the literature. They include (i) ion exchange (Olhoeft 1985), (ii) diffuse layer polarization (Dukhin & Shilov 2002), (iii) membrane polarization (Tarasov & Titov 2007), (iv) Stern layer polarization (SLP; Leroy *et al*. 2008) and (v) Maxwell–Wagner polarization (Wagner 1914; Lesmes & Morgan 2001).

Revil and collaborators have recently argued for a strong role of the SLP at low frequencies (below 1 kHz) in water-saturated sands, glass beads, sandstones and clay-rocks (Leroy *et al*. 2008; Leroy & Revil 2009). Their model has been successfully applied to connect complex conductivity to permeability (Revil & Florsch 2010), to changes in the pore water chemistry (Vaudelet *et al*. 2011a,b), and to the presence of oil in the pore space of sands (Schmutz *et al*. 2010). A simple analytical solution of this SLP model will be described in more details later in Section 2 and used to interpret experimental data (Sections 3 and 4).

The goal of our work is to provide a simple and yet accurate way to quantify the salinity dependence of complex conductivity to interpret time-lapse complex conductivity measurements in the field in association with salt tracer tests. To reach this goal, we develop a simple analytical solution of the cation sorption in the Stern layer to get a sorption isotherm. This sorption isotherm is used to predict the charge density in the Stern layer for different types of cations (Na^+ and Ca^{2+}) as a function of the salinity of the pore water solution. To the best of our knowledge, such a model has never been developed in the past. There are a number of available (published) experiments regarding the salinity dependence of the quadrature conductivity of sands and sandstones (e.g. Flath 1989; Börner 1992, 2006; Lesmes & Frye 2001; Slater & Lesmes 2002). Most of these data sets show a maximum in the trend between the quadrature conductivity versus the conductivity of the pore water solution. However, these maxima (usually located at relatively high salinities) are not consistent between the different data sets. We perform new measurements with the high-precision impedance meter described in Zimmerman *et al.* (2008, see also Cassiani *et al*. 2009) to get a high-precision data set. The development of a time-lapse inversion algorithm for complex conductivity is developed in another paper (Karaoulis *et al*. 2011). These two papers taken together offer therefore a powerful way to monitor salt tracer tests with the hope to get better results in terms of inverting the distribution of the permeability and dispersivity tensors.

2 THEORY

2.1 Macroscopic conductivity model

Several polarization mechanisms have to be considered when a silica grain is immersed in an electrolyte (in this case, an NaCl solution) and submitted to a harmonic electrical field (Fig. 1). A detailed description of these polarization mechanisms can be found in Revil & Florsch (2010) and Vaudelet *et al.* (2011a,b) (and references therein) and will not be repeated here. The SLP model implies that at low frequencies (typically below 100 Hz), the main polarization of a granular porous material with existing grain-to-grain contacts is due to the Stern layer. This model involves the migration and

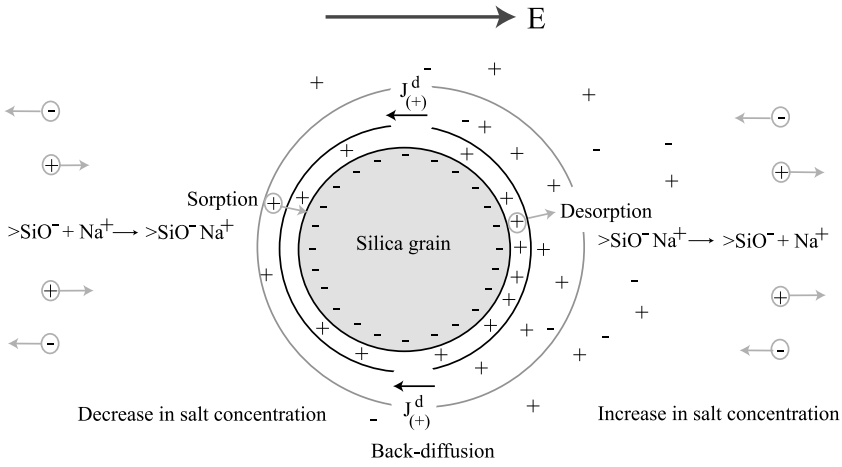

Figure 1. The presence of an applied electrical field **E** creates a dipole moment associated with the transfer of the counterions in both the Stern and the diffuse layers around a silica grain (modified from Revil & Florsch 2010). This dipole moment points in the opposite direction of the applied field. The charge attached to the mineral framework remains fixed. The movement of the counterions in the Stern layer is mainly tangential along the surface of the grain. Sorption and desorption of the counterions are in principle possible but they take time (typically few hours). Back-diffusion of the counterions (with a flux density $\mathbf{J}^d_{(+)}$) can occur both in the Stern and diffuse layers and diffusion of the salt occurs in the pore space. In both cases, the diffusion of the counterions occurs over a distance that is equal to the diameter of the grains.

accumulation of counterions on one side of the grains in the direction of the electrical field and it is assumed that the counterions have no time to sorb or desorb into or from the Stern layer. We discuss later a simple analytical solution for this model. Our motivation is to see if the SLP model can explain the dependence of the complex conductivity on salinity.

Before describing our motivations in more detail, let us first define the basic parameters describing the low-frequency complex conductivity of a porous material. We denote $\omega = 2\pi f$ the angular frequency, f the frequency (in Hertz) and $i = (-1)^{1/2}$ the pure imaginary number. The magnitude of the conductivity $|\sigma|$ and the phase lag φ are related to the real (in-phase) and imaginary (out-of-phase or quadrature) components of the complex conductivity σ^*, σ' and σ'' (expressed in S m^{-1}) by

$$\sigma^* = |\sigma| \exp(i\varphi) = \sigma' + i\sigma'' \tag{1}$$

with,

$$|\sigma| = (\sigma'^2 + \sigma''^2)^{1/2} \tag{2}$$

and,

$$\tan\varphi = \sigma''/\sigma'. \tag{3}$$

Note that some researchers use an alternative convention for the complex conductivity $\sigma^* = \sigma' - i\sigma''$, which yields a positive-defined quadrature conductivity. Induced polarization is usually displayed as a resistivity magnitude $|\rho| = 1/|\sigma|$ (in ohm m) and a phase lag φ (in rad) or alternatively as an in-phase and quadrature conductivities, σ' and σ'', respectively.

We assume for the simplicity of the presentation that we consider sand with all the grains having the same grain diameter d_0. This assumption can be relaxed using a convolution with any type of grain size distribution as shown by Revil & Florsch (2010). In the SLP model, the low-frequency complex electrical conductivity is described by a simple linear model (Revil & Florsch 2010),

$$\sigma(\omega) = \frac{1}{F}\left[\sigma_f + (F-1)\sigma_S(\omega)\right], \tag{4}$$

where $F = \phi^{-m}$ (dimensionless) is the electrical formation factor, ϕ is the connected porosity, m is the cementation exponent, σ_f (in S m^{-1}) is the conductivity of the pore water and $\sigma_S(\omega)$ is the surface conductivity. The use of eq. (4) to treat conductivity can be incorrect at low salinities as because the conductivity of a porous material is in principle a non-linear function of the conductivity of the pore water (see Bernabé & Revil 1995 for numerical simulations on synthetic porous media and Revil *et al*. 1998 for a differential effective medium approach for which eq. (4) corresponds only to a high-salinity asymptotic behaviour). That said, eq. (4) allows analytical separation of the in-phase and quadrature conductivities and is therefore very convenient for practical purposes and still a fairly good representation of reality.

The surface conductivity comprises both conduction in the diffuse and Stern layers coating the mineral surface (e.g. Kittara & Morimoto 1976). In the SLP model, the complex-valued surface conductivity is given by (Revil & Florsch 2010)

$$\sigma_S(\omega) = \frac{4}{d_0}\left(\Sigma^d + \Sigma^S\right) - \frac{4}{d_0}\frac{\Sigma^S}{1 + i\omega\tau_0}, \tag{5}$$

where $\tau_0 = d_0^2/8D_{(+)}$ is the main relaxation time (in s), $D_{(+)}$ is the diffusion coefficient of the counterions of the Stern layer coating the surface of the mineral (related to the mobility by the Nernst Einstein relationship), Σ^d is the excess of electrical conductivity in the electrical diffuse layer (called the specific surface conductivity of the diffuse layer) whereas Σ^S represents the excess of electrical conductivity in the Stern layer (called the specific surface conductivity of the Stern layer) and σ_S (in S m^{-1}) is the equivalent conductivity of the grains coated by the electrical triple layer. As a side note, Σ^d and Σ^S have dimensions of Siemens and are commonly therefore called 'conductances'. Such naming is however incorrect as they denote true surface conductivity and should therefore be called specific surface conductivities.

Eq. (5) implies that surface conductivity is characterized by a Debye relaxation mechanism with a single relaxation time. However, if this above model is convoluted with the grain size distribution (assumed to be log-normal for instance), the resulting distribution of relaxation times can be fitted with the empirical Cole–Cole model (Revil & Florsch 2010). The grain size distribution plus the effect of the roughness of the grains may explain the broad distribution of relaxation times observed in real rocks (see Vinegar & Waxman 1984; Leroy *et al*. 2008). Additional polarization mechanisms associated with the relaxation of the protons of the sorbed water (Skold *et al.* 2011) and membrane polarization (Titov *et al*. 2002) can create an even broader spectrum.

The surface conductivity can be decomposed into an in-phase component, $\sigma_{S'}(\omega)$, and a quadrature component, $\sigma_{S''}(\omega)$

$$\sigma'_S(\omega) = \sigma_S^\infty + \left(\sigma_S^0 - \sigma_S^\infty\right)\frac{1}{1+\omega^2\tau_0^2}, \tag{6}$$

$$\sigma''_S(\omega) = \left(\sigma_S^0 - \sigma_S^\infty\right)\frac{\omega\tau_0}{1+\omega^2\tau_0^2}, \tag{7}$$

$$\sigma_S^0 = \frac{4}{d_0}\Sigma^d, \tag{8}$$

$$\sigma_S^\infty = \frac{4}{d_0}\left(\Sigma^d + \Sigma^S\right), \tag{9}$$

where σ_S^0 and σ_S^∞ refer to the low and high-frequency asymptotic limits of surface conductivity, respectively. The inverse scaling between the surface conductivity and the grain diameter was demonstrated experimentally by Bolève *et al*. (2007) and Crespy *et al*. (2007). It follows that the in-phase and quadrature conductivity are given by

$$\sigma'(\omega) = \frac{1}{F}\left[\sigma_f + (F-1)\left(\sigma_S^\infty + \left(\sigma_S^0 - \sigma_S^\infty\right)\frac{1}{1+\omega^2\tau_0^2}\right)\right] \tag{10}$$

and

$$\sigma''(\omega) = \frac{F-1}{F}\left(\sigma_S^0 - \sigma_S^\infty\right)\frac{\omega\tau_0}{1+\omega^2\tau_0^2}, \tag{11}$$

respectively. Using $\tan\varphi = \sigma''/\sigma'$, the phase angle is given by

$$\varphi(\omega) = \operatorname{atan}\left[\frac{(F-1)\left(\sigma_S^0 - \sigma_S^\infty\right)\omega\tau_0}{\left(\sigma_f + (F-1)\sigma_S^\infty\right)\left(1+\omega^2\tau_0^2\right) + (F-1)\left(\sigma_S^0 - \sigma_S^\infty\right)}\right]. \tag{12}$$

Because for water-saturated porous sands and sandstones, the phase is quite small (generally smaller than 10 mrad), the phase can be approximated by the first-order Taylor expansion of the previous expression. This yields

$$\varphi(\omega) \approx \frac{(F-1)\left(\sigma_S^0 - \sigma_S^\infty\right)\omega\tau_0}{\left(\sigma_f + (F-1)\sigma_S^\infty\right)\left(1+\omega^2\tau_0^2\right) + (F-1)\left(\sigma_S^0 - \sigma_S^\infty\right)}. \tag{13}$$

This approximation is always valid for the cases investigated in this work and for field applications in absence of metallic particles like pyrite. When the surface conductivity can be neglected in the expression of the in-phase conductivity (high-salinity asymptotic behaviour), the peak phase is approximately given by

$$\varphi(\omega = 1/\tau_0) = -(F-1)\frac{\Sigma^S}{2d_0\sigma_f} \tag{14}$$

clearly indicating that the peak phase is proportional to the conductivity of the Stern layer and inversely proportional to the conductivity of the pore water as discussed recently by Vaudelet *et al*. (2011a,b). The quadrature conductivity itself is given by

$$\sigma''(\omega = 1/\tau_0) = -\left(\frac{F-1}{F}\right)\frac{\Sigma^S}{2d_0}, \tag{15}$$

so clearly the surface conductivity depends on how the salinity of the specific surface conductivity of the Stern layer varies with the salinity of the pore water, $\partial\sigma''/\partial C_f = \partial\Sigma^S/\partial C_f$, where C_f is the salinity in the pore water. As explained in the introduction, this has a huge consequence for time-lapse tomography of salt tracer tests in shallow aquifers. Note also that while eqs (14) and (15) are strictly defined at the peak frequency, usually the distribution of the relaxation times is very broad (Vinegar & Waxman 1984) and the phase and the quadrature conductivity of sandstones is observed to be weakly dependent on the frequency so the predictions of these two equations likely hold in a broad frequency range.

2.2 A Model for the specific conductivity of the Stern layer

A number of key-observations in the literature show that the quadrature conductivity is salinity-dependent. The experimental data of Börner (1992, 2006) suggest that the salinity dependence of surface conductivity is the same as the salinity dependence of the quadrature conductivity pointing out a similar mechanism (Fig. 2). This viewpoint is consistent with the vision described earlier in Section 2.1. At pH between 5 and 8, the surface of silica is covered by reactive silanol >SiOH (where > represents the crystalline framework) surface sites. We consider first a silica surface in contact with an NaCl solution. The deprotonation and sorption of sodium in the Stern layer of a silica grain can be represented by the following two reactions (e.g. Sverjensky 2005; Wang & Revil 2010):

$$> \mathrm{SiOH}^0 \Leftrightarrow > \mathrm{SiO}^- + \mathrm{H}^+, \tag{16}$$

$$> \mathrm{SiOH}^0 + \mathrm{Na}^+ \Leftrightarrow > \mathrm{SiO}^-\mathrm{Na}^+ + \mathrm{H}^+ \tag{17}$$

which correspond to the weak sorption of sodium as an outer sphere ligand, thus keeping its hydration sphere in the Stern layer. The equilibrium constants of eqs (16) and (17) are defined by

$$K_{(-)} = \frac{\Gamma^0_{\mathrm{SiO}^-}[\mathrm{H}^+]^0}{\Gamma^0_{\mathrm{SiOH}}} \tag{18}$$

and

$$K_{\mathrm{Na}} = \frac{\Gamma^0_{\mathrm{SiONa}}[\mathrm{H}^+]^0}{\Gamma^0_{\mathrm{SiOH}}[\mathrm{Na}^+]^0}, \tag{19}$$

respectively, where Γ^0_i is the surface concentration of species i in the Stern layer, $[\mathrm{H}^+]^0$ represents the concentration of protons in the Stern layer (superscript 0) and $K_{(-)} = 10^{-7.4}$ mol l^{-1} at 25 °C and K_{Na} denotes the sorption coefficient for sodium (dimensionless). Revil & Florsch (2010) simplified the formula obtained by Revil *et al*. (1999a) (see Appendix for a demonstration) and gave the following expression for the specific surface conductivity of the Stern layer:

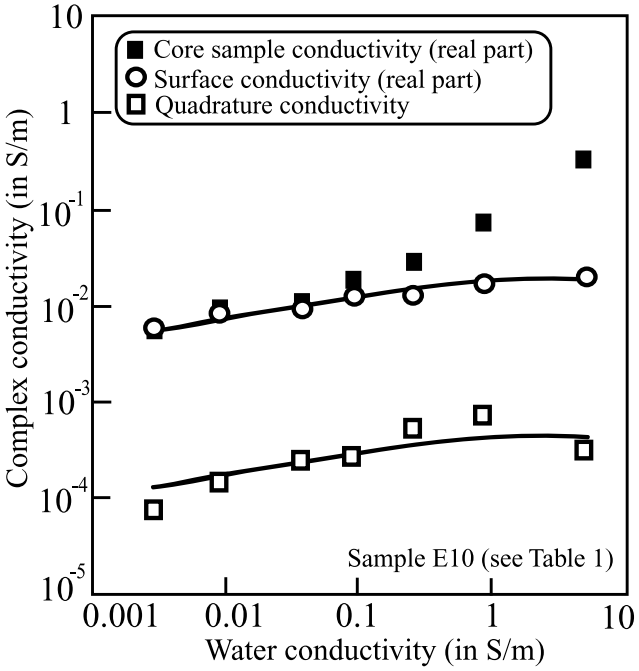

Figure 2. Experimental data showing the salinity dependence of the in phase conductivity, the surface conductivity contribution to the in-phase conductivity and the quadrature conductivity for a sandstone (modified from Börner 1992). Note that the salinity dependence of surface conductivity and quadrature conductivity seems to be the same. This may mean that the same process is at play. This process can only be understood in terms of fundamental electrochemistry of the electrical triple layer coating the pore water mineral interface. The solid lines are just guides for the eyes.

$$\Sigma^S = e\beta_{\mathrm{Na}}\Gamma^0_S\frac{K_{\mathrm{Na}}C_f}{K_{(-)} + 10^{-\mathrm{pH}} + K_{\mathrm{Na}}C_f}, \tag{20}$$

where C_f is the salinity expressed in mol l^{-1}. The total site density Γ^0_S at the surface of silica is typically on the order of 5 sites nm^{-2} (Carroll *et al*. 2002; Wang & Revil 2010) but can reach higher values (up to 10 sites nm^{-2}, see discussions in Revil *et al*. 1999a,b). Hiemstra & Van Riemsdijk (1990) used $\Gamma^0_S = 9.6$ sites nm^{-2} for the (001) crystalline plane of silica and $\Gamma^0_S = 6.0$ sites nm^{-2} for the (101) crystalline plane. A site density of 5 sites nm^{-2} yields $e\,\Gamma^0_S = 0.8$ C m^{-2}. Using these values and reasonable values for the mobility of the counterions (see below), we can compute the dependence of the specific surface conductance of the Stern layer on salinity. We should keep in mind that eq. (20) has many limitations: (1) it is only valid for a narrow pH range (from 5 to 8) and (2) it is an approximation of much more complex triple layer models (TLMs) (see Wang & Revil 2010; Vaudelet *et al*. 2011a,b, Skold *et al*. 2011 for instance and references therein). So eq. (20) should be considered a semi-empirical relationship rather than a fully theoretically justified model. That said, we will see that this relationship agrees with the data. The combination of eqs (15) and (20) yields a close-form relationship between the quadrature conductivity, the salinity and the grain diameter

$$\sigma'' = -\left(\frac{F-1}{F}\right)\left(\frac{e\beta_{\mathrm{Na}}\Gamma^0_S}{2d_0}\right)\frac{K_{\mathrm{Na}}C_f}{K_{(-)} + 10^{-\mathrm{pH}} + K_{\mathrm{Na}}C_f}. \tag{21}$$

Note that for the cases investigated below $K_{(-)} << 10^{-\mathrm{pH}}$ and the term $K_{(-)}$ can therefore be neglected in eq. (21). To our knowledge, this is the first time that such a direct analytical relationship is

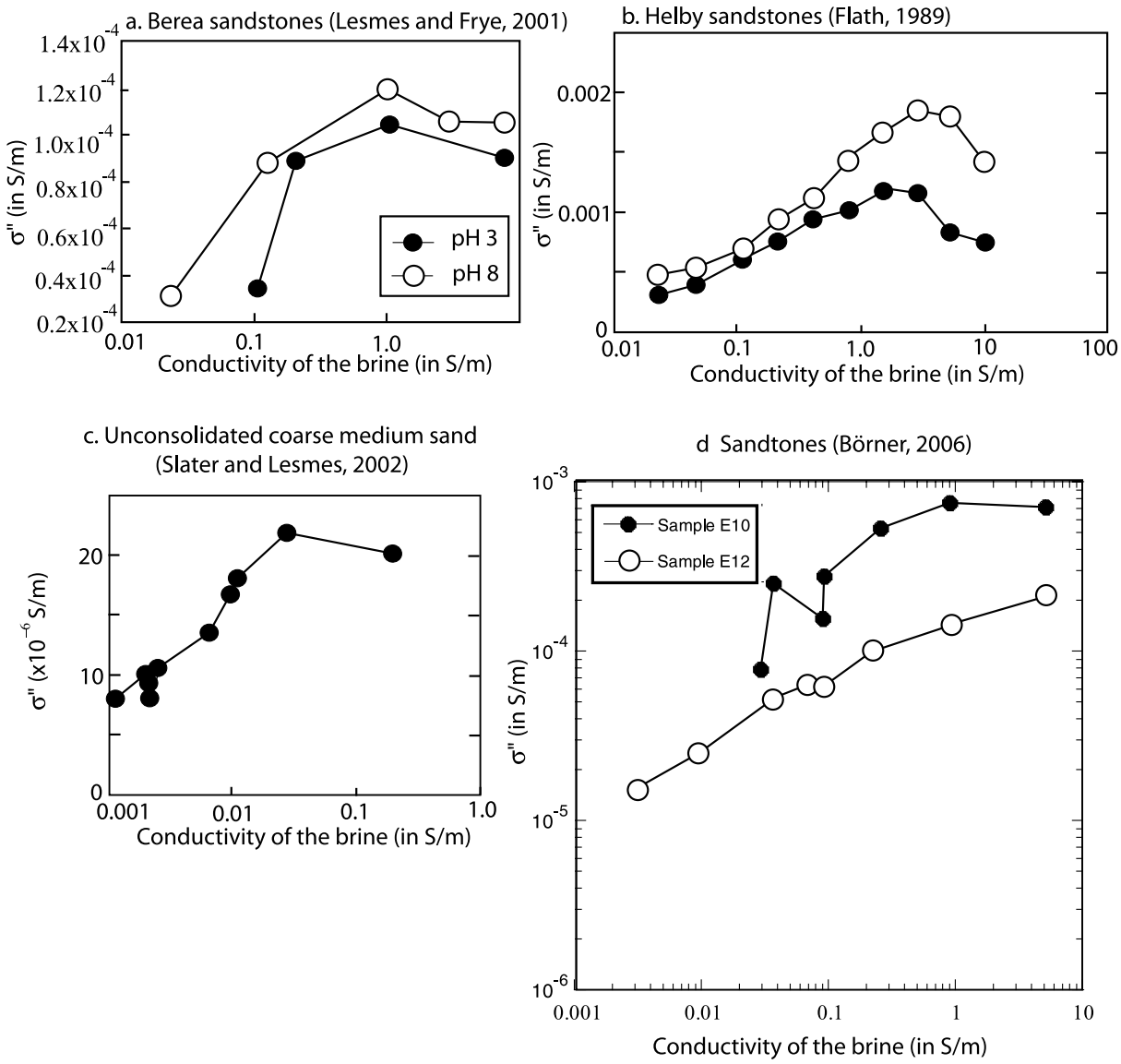

Figure 3. Salinity dependence of the quadrature conductivity. (a) Berea sandstone (Lesmes & Frye 2001). (b) Helby sandstones (Flath 1989). (c) Unconsolidated coarse medium sand (Slater & Lesmes 2002, sample G1, 1 Hz, 200 μm from permeability and formation factor estimates of table 1). (d) Börner (1992, 2006), sandstones (see Table 1). The lines are guides for the eyes. Note that for some samples, the decrease of the quadrature conductivity at high salinities may be due to membrane polarization.

obtained. Revil *et al*. (1999a) considered that $K_{\rm Na} = 10^{-3.25}$ at 25°C from titration experiments (Revil *et al*., 1999a, their fig. 2) at pH = 6. The mobility of sodium in the pore water is $\beta_{\rm Na} = 5.19\times 10^{-8}$ m^{2}s^{-1}V^{-1} (25 °C). We assume that the mobility of sodium in the Stern layer remains unchanged with respect to its value in the bulk pore water. However, this assumption is also questionable and we will see later that some data sets can only be modelled with a lower (by a factor 2.5) mobility.

In the case of a divalent cation like Ca^{2+}, the same type of relationship can be obtained. This yields

$$\Sigma^S = 2e\beta_{\rm Ca}\Gamma_S^0 \frac{K_{\rm Ca}C_f}{10^{-\rm pH} + K_{\rm Ca}C_f}, \tag{22}$$

$$\sigma'' = -\left(\frac{F-1}{F}\right)\left(\frac{e\beta_{\rm Ca}\Gamma_S^0}{d_0}\right)\frac{K_{\rm Ca}C_f}{10^{-\rm pH} + K_{\rm Ca}C_f}, \tag{23}$$

where $K_{\rm Ca}$ is the equivalent equilibrium constant corresponding to the sorption reaction for calcium. Interestingly, the high-salinity plateau yields direct information on the mobility of the counterions. Indeed, the ratio of eqs. (21) and (23) yields

$$\frac{\sigma''({\rm Na})}{\sigma''({\rm Ca})} = \frac{\beta_{\rm Na}}{2\beta_{\rm Ca}}. \tag{24}$$

This equation will be used in Section 3 to determine the mobility of calcium in the Stern layer.

Finally, one may want to correct the quadrature conductivity for the effect of temperature. The specific surface conductivity can be corrected for temperature according to (Revil *et al*. 1999b).

$$\Sigma^S(T) = \Sigma^S(T_0)\left(1 + \alpha_S(T - T_0)\right). \tag{25}$$

In Eq. (18), the temperature is expressed in °C, $T_0 = 25$ °C, and the linear temperature sensitivity coefficient α_S is between 0.020

and 0.040 $^{\circ}C^{-1}$. According to eq. (15), the quadrature conductivity should then increase with the temperature as

$$\sigma''(T) = \sigma''(T_0)(1 + \alpha_S(T - T_0)) . \quad (26)$$

Eq. (26) can be used to correct temperature variations (especially for a less than 5 $^{\circ}$C range as observed in laboratory conditions). The pore water conductivity depends on temperature according to

$$\sigma_f(T) = \sigma_f(T_0)\left(1 + \alpha_f(T - T_0)\right), \quad (27)$$

where the linear temperature sensitivity coefficient α_f ranges from 0.019 to 0.023 $^{\circ}C^{-1}$. Using eqs (14), (26) and (27) at high salinities (for which surface conductivity can be neglected in the in-phase conductivity), we have

$$\varphi(T) = \varphi(T_0)\left(1 + (\alpha_S - \alpha_f)(T - T_0)\right) \quad (28)$$

to the first order in the temperature disturbance $\delta T = T - T_0$. According to eq. (28), the phase is therefore expected to be weakly dependent on temperature in agreement with the experimental data reported in Vinegar & Waxman (1984, their fig. 14).

3 MEASUREMENTS

In the following, we perform new measurements with the high-precision impedance meter described in Zimmerman *et al.* (2008) (see also Cassiani *et al*. 2009). To test the accuracy of this apparatus, we performed first some measurements on two known electrical RC circuits (see Fig. 4) with two very different values of the resistance and the capacitance. In both cases, it seems that the phase is accurate at least down to 0.1 mrad.

The experiments were realized with two fully saturated sands. The Uminin #30 sand has a grain diameter of 350 μm with angular grains whereas sand B has a mean grain size of 175 μm (the grain sizes are between 150 and 210 μm) with spherical silica grains (Silica Spherical 7030 from Charles B. Chrystal Co. Inc., Mamaroneck, NY, USA; www.cbchrystal.com, 99.5 per cent SiO_2). Their properties (porosity, permeability and formation factors) are reported in Table 1 together with some additional data from other samples investigated in the literature and discussed later in Section 5. We performed SIP measurements on the Unimin #30 sand using the type of tank described in Fig. 5. A lid was used to minimize evaporation. The plastic tanks were 29 cm long and 18 cm wide and were packed with 6000 g of sand and 1850 g aqueous solution resulting in a sand depth of approximately 7.5 cm. The sand was packed wet to avoid trapping air bubbles. The wet sand was compacted for 75 min at 8.3 kPa resulting in a final volume of approximately 3.85 l and a porosity of 41 per cent. Four non-polarizing Pb-$PbCl_2$, electrodes were inserted 2 cm into the sand in a rectangular array with 8 and 10.5 cm long sides throughout the experiment. In this tank, the geometrical factor was measured experimentally to 0.28 m using a controlled sand experiment with known electrolyte conductivities.

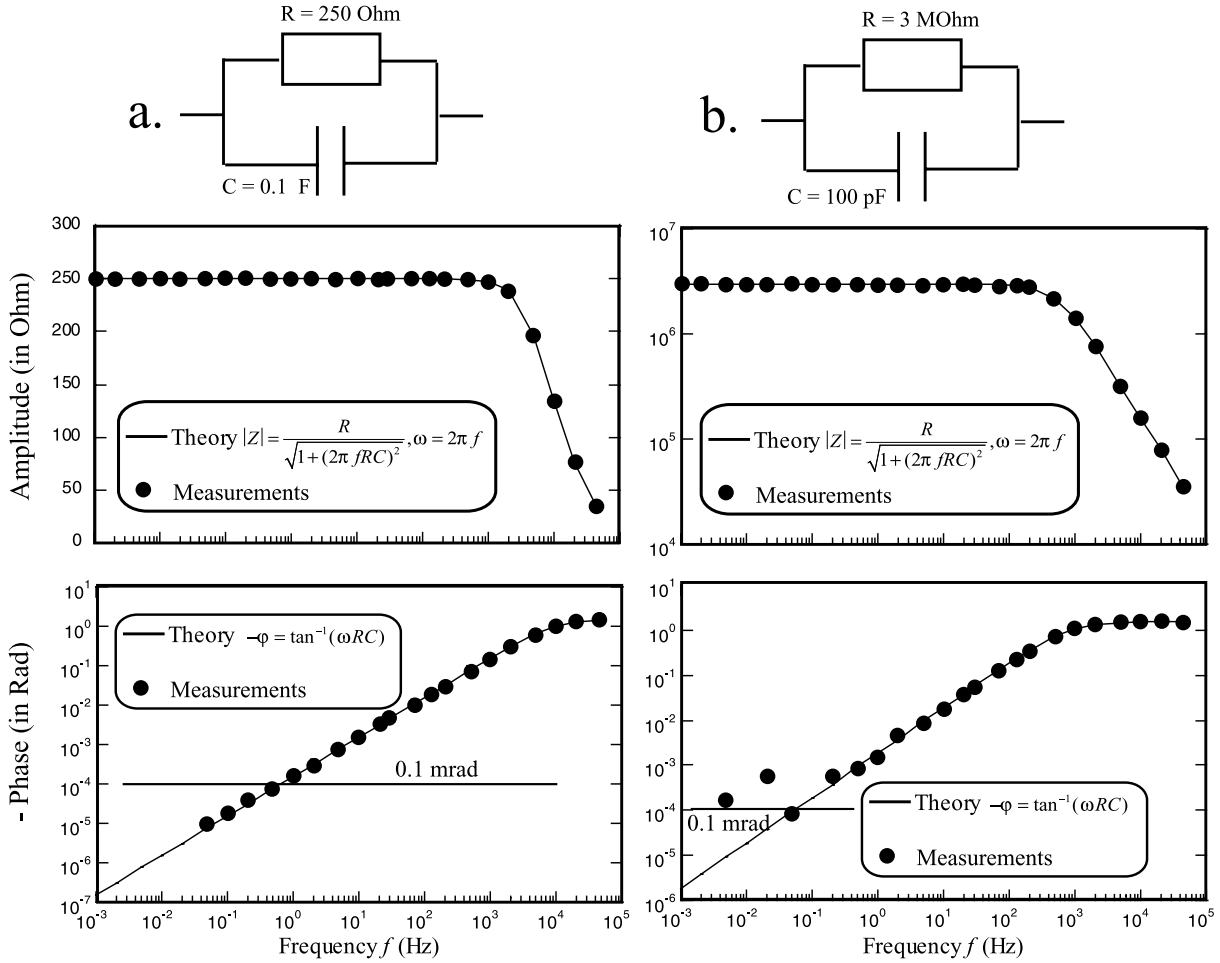

Figure 4. Test of the sensitivity of the impedance meter used in our experiments. We test the impedance meter by measuring the impedance of a known resistance in parallel to a known capacitance. (a) Test with a low resistance of 250 ohm and a high capacitance 0.1 F. (b) Test with a high resistance of 3 Mohm and a small capacitance of 100 pF.

Table 1. Petrophysical properties of the samples used in this study to evaluate the SLP model. F represents the formation factor and k the permeability.

Sample	Nature	Porosity ϕ (-)	F(-)	k (m^2)	m^f (-)	d_0 (μm)
E10[a]	Saxony Sandstone	0.224	17.0	5.4×10^{-15}	1.89	52
E12[a]	Saxony Sandstone	0.259	11.0	1.49×10^{-12}	1.09	250
U30[b]	Silica sand	0.41	3.6	2.47×10^{-10}	1.44	350
Sand B[c]	Silica sand	0.33	3.7	1.01×10^{-10}	1.18	175
Berea[d]	Berea sandstone	0.18	15.9	2.28×10^{-13}	1.61	260
G1[e]	Sand with silt	0.33	4.3	2×10^{-11}	1.32	260

Notes:
[a]Börner (1992).
[b]This work (Uminin #30, grain diameter 350 μm).
[c]This work (grain diameter 175 μm).
[d]Lesmes & Frye (2001).
[e]Slater & Lesmes (2002).
[f]Using Archie's law $m = -\ln(F)/\ln(\phi)$.

Experiments using acid-washed sand B were performed in a cylindrical Teflon container with a diameter of 7.3 cm and a sand filled depth of 10.8 cm. The pH was adjusted using NaOH to neutralize small amounts of HCl left in the sand. Ag(s)/AgCl electrodes with a diameter of 2 mm were inserted 1 cm into the sand in a rectangle array with sides 2.5 and 5.0 cm. The geometrical factor was measured to 0.096 m using similar experiments to the large tank experiments. In both setups, the sand-filled containers were left for 5 d and the SIP response was measured at several times to assure that the electrical properties of the porous media were stable.

Aqueous solutions were made by dissolving NaCl or $CaCl_2$ (Aldrich, ACS; www.sigmaaldrich.com) into deionized water. The pH of the NaCl solutions was adjusted with sodium hydroxide (Mallinckrodt Chemicals, ACS; Phillipsburg, NJ, USA) or hydrochloric acid (EMD Chemicals, ACS; Gibbstown, NJ, USA) prior to preparing the tanks. Experiments aimed at investigating the effect of NaCl concentration on the SIP response were performed at initial pH of 6.2 and the NaCl concentration of the pore water.

A typical spectrum for the phase is shown in Fig. 6. The in-phase conductivity (not shown) is nearly frequency-independent indicating the weak role of the (frequency-dependent) surface conductivity. The spectrum shown in Fig. 6 exhibits a low-frequency polarization possibly associated with the polarization of the electrical triple layer or possibly with membrane polarization. According to the SLP model, the low-frequency polarization is due to the polarization of the Stern layer (Leroy *et al*. 2008; Revil & Florsch 2010). We also observe an increase of the phase lag above 100 Hz. This increase of the phase lag is associated with the dielectric (Maxwell–Wagner) polarization (Leroy *et al*. 2008). The entire data set is shown in Fig. 7. According to Archie's law for the Unimin #30 and for Sand B, the electrical formation factor can be described by $F = \phi^{-m}$ with $m = 1.3$–1.5. This yields a formation factor of 3.2–3.8 with a mean value of $F = 3.5$. This estimate is in agreement with the measured value of 3.7 (see Fig. 7b). In Section 4, we compare our results to the SLP theory.

4 THEORY VERSUS EXPERIMENTAL DATA

4.1 Peak frequency

Let us first test the theory with the low-frequency data set taken as an example in Fig. 6. According to the SLP model, the relaxation frequency (in Hertz) corresponding to the peak of the quadrature conductivity is defined as

$$f_0 = \frac{\omega_0}{2\pi} = \frac{1}{2\pi\,\tau_0}, \tag{29}$$

where the expression of the relaxation time τ_0 is given just below eq. (5) above. Taking $d_0 = 350$ μm, $D_{(+)} = 1.32\times10^{-9}$ m^2 s^{-1} for Na^+ at 25 °C (e.g. Vaudelet *et al*. 2011a, their table 4), the loss peak f_0 occurs at ∼14 MHz ($\tau_0 = 71$ s) in good agreement with the data (Fig. 6). The peak phase is given by eq. (14) and should be quite independent on the salinity. Considering eq. (14) and taking the measured conductivity value of $\sigma_f = 0.29$ S m^{-1} (and therefore $\Sigma^S = 4\times10^{-8}$ S according to the model described earlier, eq. 22), $F = 3.7$, $d_0 = 350$ μm, the peak of the phase lag is –0.53 mrad ($\log_{10}$ phase = –3.2). The measured value is $\log_{10}$ phase = –3.1

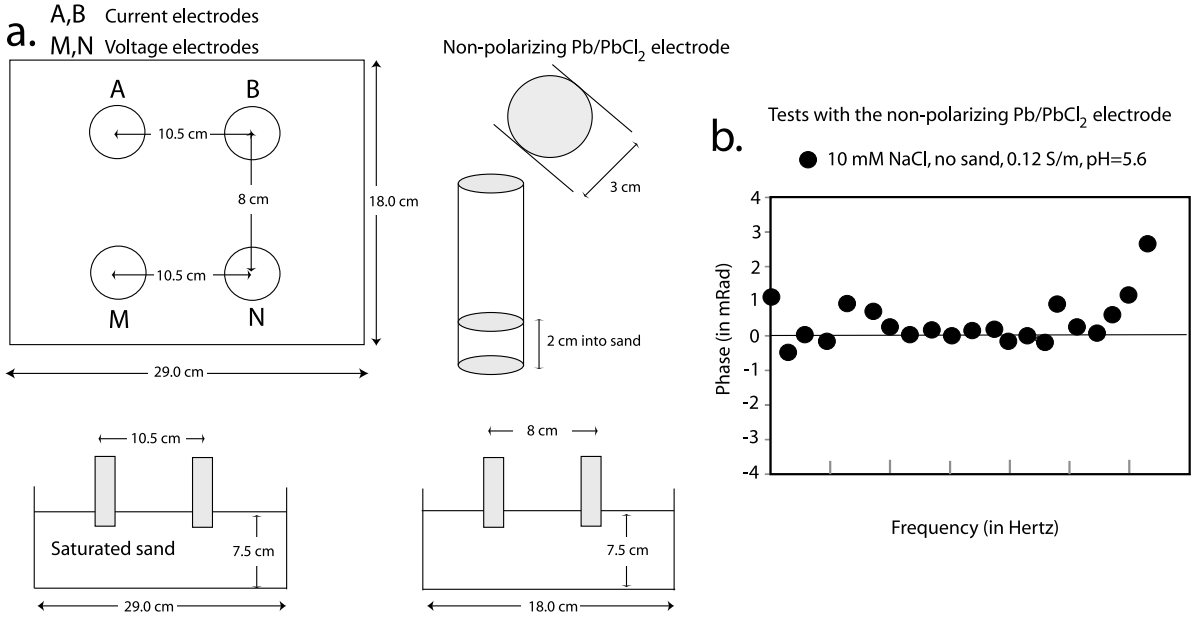

Figure 5. Experimental setting used to measure the complex resistivity. (a) The electrodes are non-polarizing $Pb/PbCl_2$ electrodes. They are used as current electrodes (A and B) and potential electrodes (M and N). The tank is made of plastic. (b) Test of the phase accuracy in absence of sand in an NaCl electrolyte.

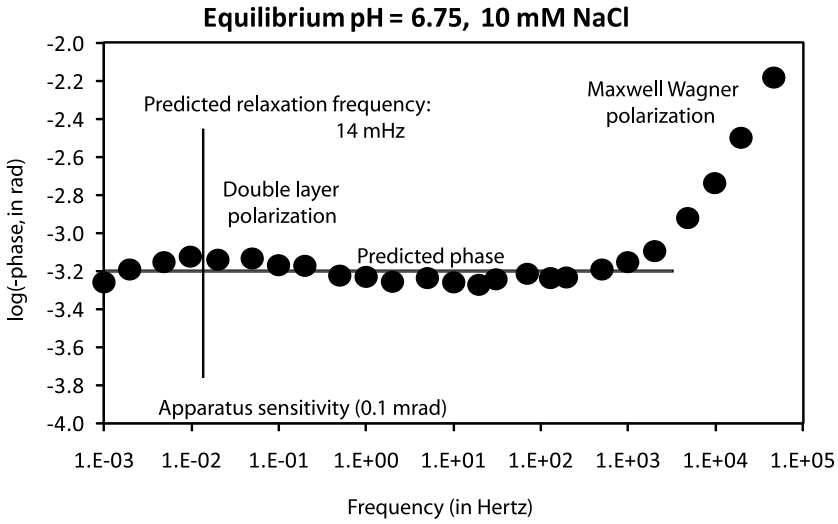

Figure 6. Example of phase data recorded over the full spectrum of frequencies (1 MHz to 40 kHz). The data exhibit clearly two polarization relaxations. The relaxation observed at low frequencies has been recently associated to the polarization of the Stern layer whereas the one at high frequencies is associated with the Maxwell–Wagner polarization.

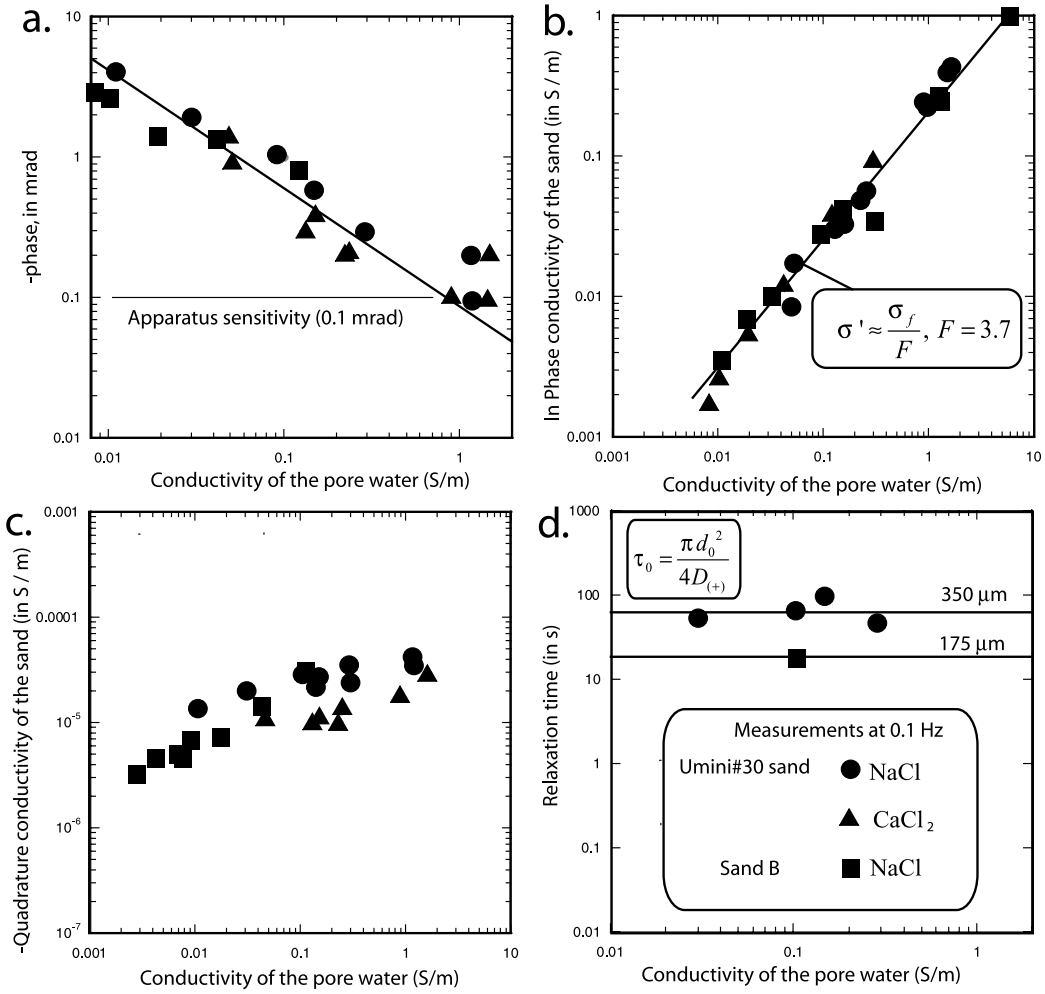

Figure 7. Phase and in-phase conductivity versus the conductivity of the pore water for the Umini#30 sand (350 µm, 0.1 Hz). (a) Phase versus brine conductivity. The straight line indicates an inverse relationship between the quadrature conductivity and the conductivity of the pore water showing that the effect of the salinity upon the phase is dominated by the influence of the salinity upon the in-phase conductivity. (b) In-phase conductivity of the sand versus the conductivity of the pore water. The linear trend is used to estimate the intrinsic formation factor F neglecting the effect of the surface conductivity because of the coarse size of the grains. (c) Quadrature conductivity versus the conductivity of the pore water. (d) Main relaxation time versus conductivity of the pore water.

(Fig. 6). Therefore, there is a fair agreement between the theory and the experimental data.

4.2 Mobility of the counterions in the stern layer

Regarding the pore water conductivity dependence of the quadrature conductivity in isothermal conditions (25 °C), there is agreement between the data and the model (Fig. 8a).

From the observed dependence of the observed plateau on the electrolyte (data sets with NaCl and $CaCl_2$ solutions, see Fig. 8b), we deduce that the mobility of calcium β_{Ca} is approximately four times smaller than the mobility of sodium. This ratio has been reported by Revil *et al*. (1998, their table 1) from surface conductivity measurements indicating, once more, that there is a direct relationship between the surface conductivity and the quadrature conductivity.

4.3 Salinity dependence of the specific surface conductivity

An alternative way to check the theory is to compute the salinity dependence of the specific surface conductivity from the quadrature conductivity data (Fig. 7). Combining eq. (11) with eqs (8) and (9), the specific surface conductivity scales with the quadrature conductivity as

$$\Sigma^S\left(\sigma_f^1\right) = \Sigma^S\left(\sigma_f^2\right)\frac{\sigma''\left(\sigma_f^1\right)}{\sigma''\left(\sigma_f^2\right)}, \tag{30}$$

where σ_f^1 and σ_f^2 are two different conductivities of the pore waters. We use this expression to scale the quadrature conductivity data from our measurements and those reported in the literature (see Fig. 9). Therefore, we normalize the value of the quadrature conductivities with respect to the value reached by the quadrature conductivity of 1 S m^{-1}, and we compute the value of the

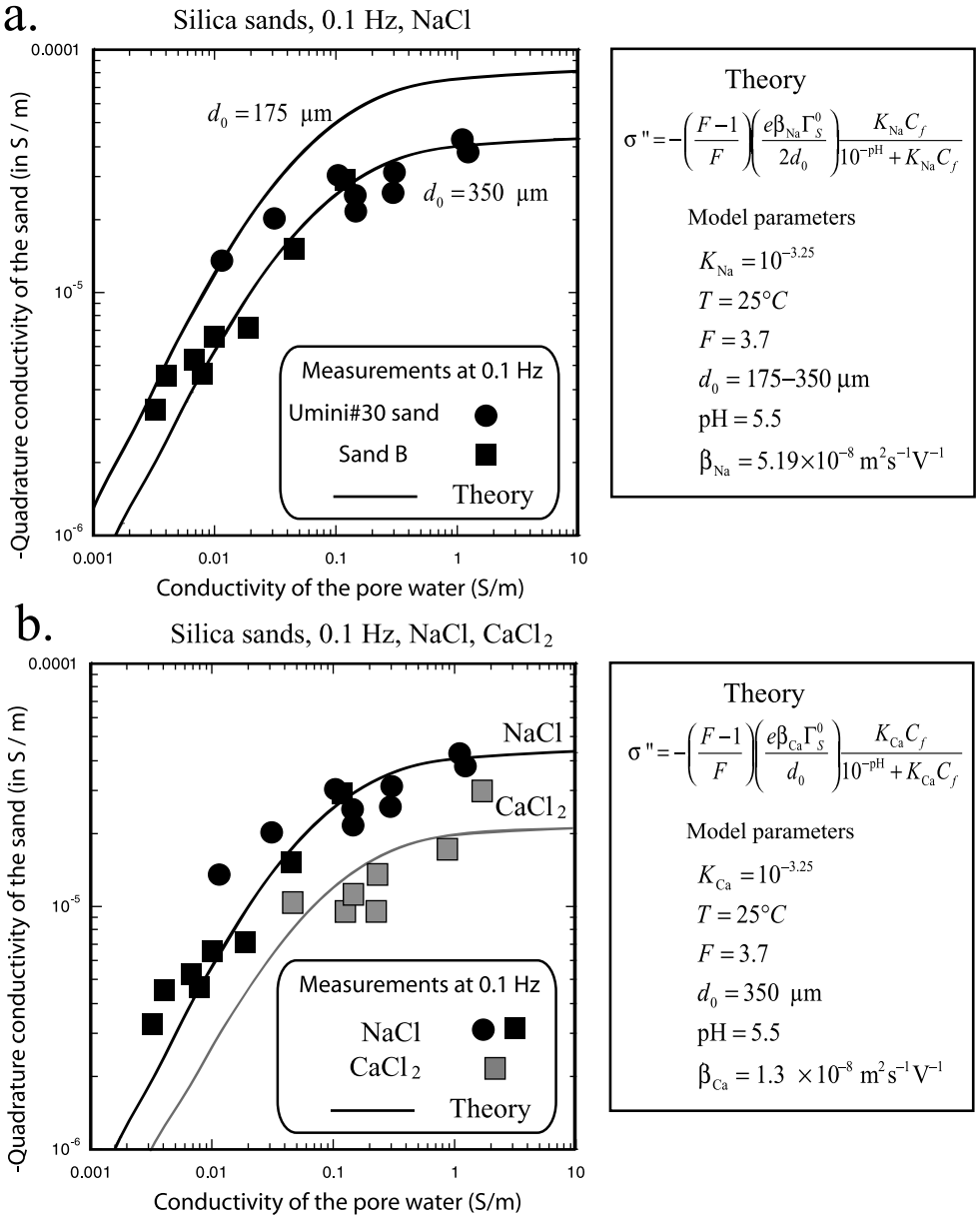

Figure 8. Comparison between the experimental data for the quadrature conductivity and the prediction of the model. Note that all the parameters entering into the model are fixed through independent estimates (listed on the lower left corner). The total site density is 5 sites per nm^2. (a) For a sodium chloride solution. (b) Comparison with a $CaCl_2$ solution.

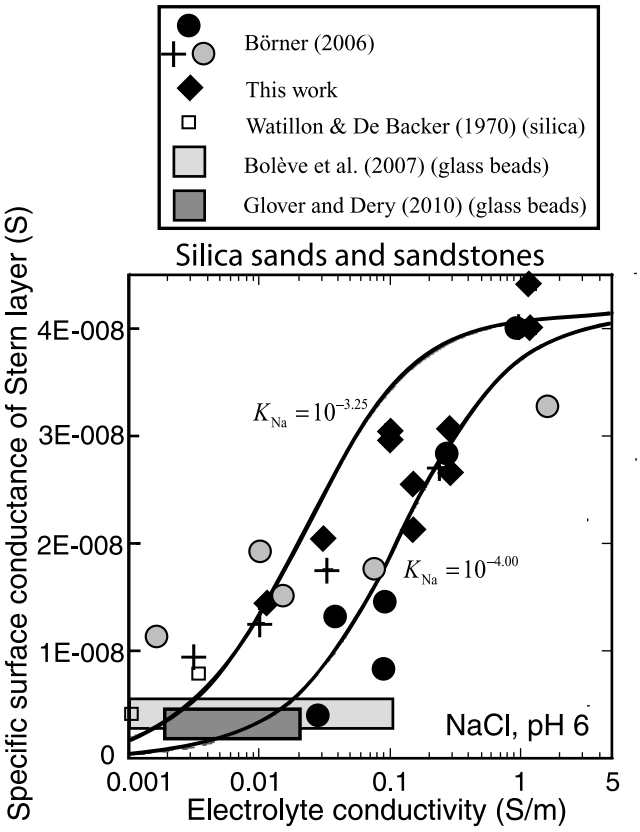

Figure 9. Specific surface conductivity of the Stern layer: comparison between the analytical model discussed in the main text and the experimental data (normalized quadrature conductivities and direct estimates). The model (25 °C, NaCl, plain line) is shown for two values of the sorption coefficient of sodium in the Stern layer.

corresponding specific conductivity using the model described in Section 2 for two values of the sorption equilibrium constant for sodium (Fig. 9). An excellent comparison is obtained in terms of trends. Indeed, the measured quadrature conductivities scale with the salinity like the specific surface conductivity of the Stern layer scales with the salinity in our model.

4.4 Additional tests

Now that we have a useable and tested expression for the specific surface conductivity of the Stern layer as a function of the salinity, we can test if the SLP model is able to predict the quadrature conductivity of sands and sandstones of additional data sets. In Figs 10 and 11, we test the validity of eq (33) with the values of the specific surface conductivity predicted by eq. (20). Usually, the grain diameter is not known and it can be replaced by an expression related to the permeability and to the formation factor (see Revil & Florsch 2010). The quadrature conductivity is given by eq. (15) and is therefore directly proportional to the specific surface conductivity of the Stern layer. The permeability is related to the grain diameter by (Revil & Florsch 2010, their eq. 14, modified from Revil & Cathles 1999)

$$k = \frac{d_0^2}{32m^2 (F-1)^2 F}. \tag{31}$$

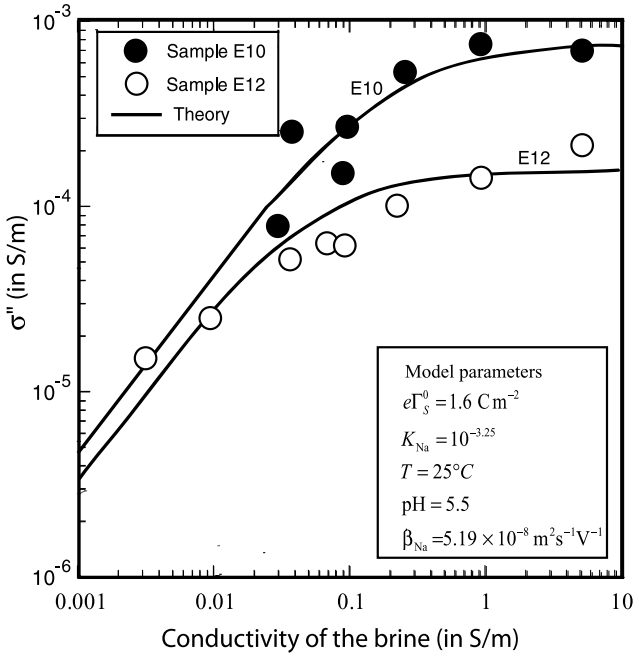

Figure 10. Test of the SLP model. The input parameters for the predicted quadrature conductivity are the measured permeability, the measured formation factor and the value of the specific surface conductivity of the Stern layer (at 25 °C) computed from the analytical model.

In eqn. (31), m is the cementation exponent of Archie's law. Therefore, the mean grain diameter is related to the permeability by

$$d_0 = m(F-1)\sqrt{32kF}. \tag{32}$$

Therefore, the quadrature conductivity can be related to the permeability and to the formation factor by the following relationship:

$$\sigma''(\omega = 1/\tau_0) = -\frac{\Sigma^S}{8m\sqrt{2kF^3}}. \tag{33}$$

In Fig. 10, we compare the predictions of our model with the samples investigated by Börner (1992, 2006,see properties in Table 1). There is fair agreement between the prediction of our model and the salinity dependence of the quadrature conductivity. In Fig. 11, we perform a test of the SLP model with the data of Slater & Lesmes (sample G1, see table 2). The mean grain size $d_0 = 230$ μm is estimated from the measured permeability $k = 2\times10^{-11}$ m^2 of Sample G1 from Slater & Lesmes (2002) and the measured formation factor ($F = 4.3$). There is good agreement between the model prediction and the experimental data.

5 CONCLUSIONS

Based on a new set of experimental data and the development of an analytical solution regarding the salinity and type of cation dependence of quadrature conductivity, the following two conclusions have been reached:

(1) The quadrature conductivity of sands and sandstones increases with the salinity of NaCl and $CaCl_2$ solutions until a constant value is reached above 1 S m^{-1}.

(2) The dependence of the quadrature conductivity on salinity of a NaCl solution can be explained by a polarization model of the Stern layer, which corresponds to the inner part of the electrical triple layer coating the surface of the grains. This approach shows that the specific surface conductivity of the Stern layer increases

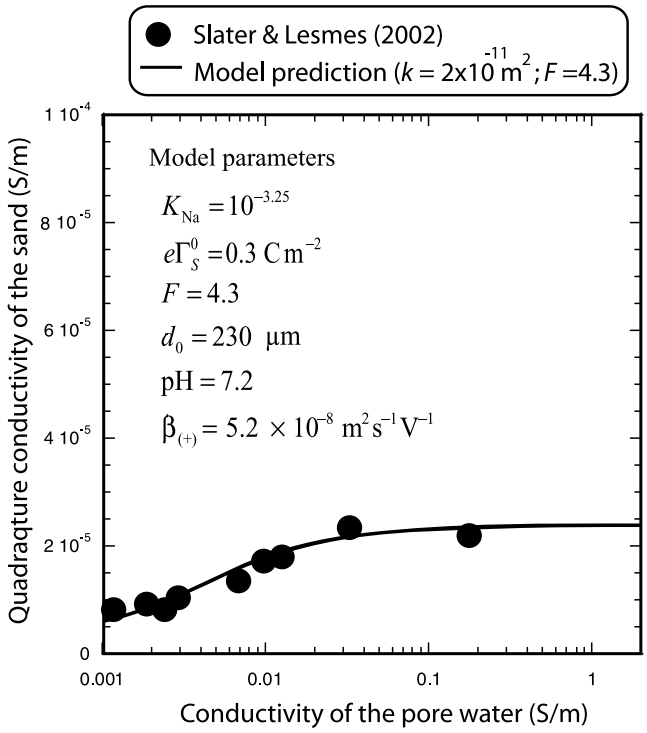

Figure 11. Tests of the Stern layer model. The input parameters for the predicted quadrature conductivity are the measured formation factor and the value of the specific surface conductivity of the Stern layer (at 25 °C).

with the salinity as a result of the increase of the population of counterions weakly sorbed in the Stern layer.

The present model is the first step in obtaining an accurate model that describes the salinity dependence of both the in-phase and quadrature components of the electrical conductivity of silica sands and sandstones. This model still needs to be completed for clays and therefore for shaly sandstones. Our model could be used to interpret time-lapse SIP tomography associated with the injection of a salt tracer in a heterogeneous aquifer made of silica sands and sandstones. This work is complementary to the development of a time-lapse inversion algorithm for SIP data. Such algorithm is developed in another paper (Karaoulis *et al*. 2011). The use of induced polarization to monitor salt tracer test data could be combined with recent efforts in analysing self-potential data associated with the migration of a salt plume in a sandy aquifer (Revil & Jardani 2010). The joint inversion of time-lapse induced polarization and self-potential data could be a powerful approach in monitoring salt tracer tests and contaminant plumes.

ACKNOWLEDGMENTS

We thank the National Science Foundation (NSF award CMMI 0926276 and NSF EAR-0711053) and the Office of Science (BER), US Department of Energy (award DE-FG02–08ER646559) for financial supports. We thank Lee Slater for illuminating discussions and Egon Zimmermann for the quality of his impedance meter. We thank Andreas Weller and an anonymous referee for their very constructive and useful reviews.

REFERENCES

Atekwana, A. & Slater, L., 2009. Biogeophysics: a new frontier in Earth science research, *Rev. Geophys.,* **47,** RG4004, doi:10.1029/2009RG000285.

Bernabé, Y. & Revil, A., 1995. Pore-scale heterogeneity, energy dissipation and the transport properties of rocks, *Geophys. Res. Lett.,* **22**(12), 1529–1552.

Binley, A. & Kemna, A., 2005. DC resistivity and induced polarization methods, in *Hydrogeophysics,* Chapter **5**, pp. 129–156, eds Rubin, Y. & Hubbard, S., Springer, The Netherlands.

Bolève, A., Crespy, A., Revil, A., Janod, F. & Mattiuzzo, J. L., 2007. Streaming potentials of granular media: influence of the Dukhin and Reynolds numbers, *J. geophys. Res.,* **112,** B08204, doi:10.1029/2006JB004673.

Börner, F.D., 1992. Complex conductivity measurements of reservoir properties, in *Proceedings of the Third European Core Analysis Symposium,* Paris, pp. 359–386.

Börner, F.D., 2006. Complex conductivity measurements, in *Groundwater Geophysics,* 119–153, doi: 10.1007/3-540-29387-6_4.

Carroll, S., Maxwell, R.S., Bourcer, W., Martin, S. & Hulsey, S., 2002. Evaluation of silica-water surface chemistry using NMR spectroscopy, *Geochim. Cosmochim. Acta,* **66**(6), 913–926.

Cassiani, G, Kemna, A., & Villa, A., 2009. Spectral induced polarization for the characterization of free-phase hydrocarbon contamination of sediments, *Near Surf. Geophys.,* **7**(5–6), 547–562.

Cole, K.S. & Cole, R.H., 1941. Dispersion and absorption in dielectrics. I. Alternating current characteristics, *J. Chem. Phys.,* **9,** 341–351.

Crespy, A., Bolève, A. & Revil, A., 2007. Influence of the Dukhin and Reynolds numbers on the apparent zeta potential of granular porous media, *J. Coll. Interface Sci.,* **305,** 188–194.

Dukhin, S.S. & Shilov, V.N., 2002. Non-equilibrium electric surface phenomena and extended electrokinetic characterization of particles, in *Interfacial Electrokinetics and Electrophoresis,* Surfactant Science Series, Vol. **106**, pp. 55–85, ed. Delgado, A.V., Marcel Dekker, New York.

Flath, D., 1989. The low-frequency complex electrical response of brine saturated shaly sandstones, *Ph.D. thesis*. University of Birmingham, Birmingham, UK.

Glover, P.W.J. & Dery, N., 2010. Streaming potential coupling coefficient of quartz glass bead packs: dependence on grain diameter, pore size, and pore radius, *Geophysics,* **75**(6), F225–F241.

Hiemstra, T. & Van Riemsdijk, W.H. 1990. Multiple activated complex dissolution of metal (hydr)oxyde: a thermodynamic approach applied to quartz, *J. Coll. Interface Sci.,* **136,** 132–150.

Hördt, A., Blaschek, R., Kemna, A. & Zisser, N., 2007. Hydraulic conductivity estimation from induced polarisation data at the field scale—the Krauthausen case history, *J. appl. Geophys*., **62,** 33–46.

Jardani, A. *et al*., 2009. Reconstruction of the water table from self potential data: a Bayesian approach, *Ground Water,* **47**(2), 213–227.

Karaoulis M., Revil A., Werkema D.D., Minsley B., Woodruff W.F. & Kemna A., 2011. Time-lapse 3D inversion of complex conductivity data using an active time constrained (ATC) approach, *Geophys. J. Int.,* **187,** 237–251, doi:10.1111/j.1365-246X.2011.05156.

Kemna, A., 2000. Tomographic inversion of complex resistivity: theory and application, *PhD thesis*. Bochum University, 196pp.

Kemna, A., Münch, H.-M., Titov, K., Zimmermann, E. & Vereecken, H., 2005. Relation of SIP relaxation time of sands to salinity, grain size and hydraulic conductivity, in *Proceedings of the 11th European Meeting of Environmental and Engineering Geophysics,* Extended Abstracts: Near Surface 2005, P054.

Kittara, S. & Morimoto, T., 1976. Surface conductance of silica in electrolyte solutions, *J. Coll. Interface Sci.,* **55**(2), 431–439.

Leroy, P. & Revil, A., 2009. A mechanistic model for the spectral induced polarization of clay material, *J. geophys. Res.,* **114,** B10202, doi:10.1029/2008JB006114.

Leroy, P., Revil, A., Kemna, A., Cosenza, P. & Ghorbani, A., 2008. Spectral induced polarization of water-saturated packs of glass beads, *J. Coll. Interface Sci.,* **321**(1), 103–117.

Lesmes, D.P. & Frye, K.M., 2001. Influence of pore fluid chemistry on the complex conductivity and induced polarization responses of Berea sandstone, *J. geophys. Res*., **106**(B3), 4079–4090.

Lesmes, D.P. & Morgan, F.D., 2001. Dielectric spectroscopy of sedimentary rocks, *J. geophys. Res*., **106** (B7), 13 329—13 346.

de Lima, O.A.L. & Niwas, S., 2000. Estimation of hydraulic parameters of shaly sandstone aquifers from geoelectrical measurements, *J. Hydrol.,* **235,** 12–26, doi:10.1016/S0022-1694(00)00256-0.

Müller, K., Vanderborght, J., Englert, A., Kemna, A., Huisman, J.A., Rings, J. & Vereecken, H., 2010. Imaging and characterization of solute transport during two tracer tests in a shallow aquifer using electrical resistivity tomography and multilevel groundwater samplers, *Water Resour. Res.,* **46,** W03502, doi:10.1029/2008WR007595.

Olhoeft, G. R., 1985. Low-frequency electrical properties, *Geophysics,* **50,** 2492–2503.

Pollock, D. & Cirpka, O.A., 2008. Temporal moments in geoelectrical monitoring of salt tracer experiments, *Water Resour. Res.,* **44,** W12416, doi:10.1029/2008WR007014.

Revil, A. & Cathles, L.M., 1999. Permeability of shaly sands, *Water Resour. Res*., **35**(3), 651–662.

Revil, A. & Florsch, N., 2010. Determination of permeability from spectral induced polarization data in granular media, *Geophys. J. Int.,* **181,** 1480–1498, doi:10.1111/j.1365-246X.2010.04573.x.

Revil, A. & Jardani, A., 2010. Stochastic inversion of permeability and dispersivities from time lapse self-potential measurements: a controlled sandbox study, *Geophys. Res. Lett.,* **37,** L11404, doi:10.1029/2010GL043257.

Revil, A., Cathles, L.M., Losh, S. & Nunn, J.A., 1998. Electrical conductivity in shaly sands with geophysical applications, *J. geophys. Res.,* **103**(B10), 23 925–23 936.

Revil, A., Pezard, P.A. & Glover, P.W.J., 1999a. Streaming potential in porous media. 1. Theory of the zeta-potential, *J. geophys. Res.,* **104**(B9), 20 021–20 031.

Revil, A., Schwaeger, H., Cathles, L.M. & Manhardt, P., 1999b. Streaming potential in porous media. 2. Theory and application to geothermal systems, *J. geophys. Res.,* **104**(B9), 20 033–20 048.

Schmutz, M., Revil, A., Vaudelet, P., Batzle, M., Femenía Viñao, P. & Werkema, D.D., 2010. Influence of oil saturation upon spectral induced polarization of oil bearing sands, *Geophys. J. Int.,* **183,** 211–224, doi:10.1111/j.1365-246X.2010.04751.x.

Singha, K. & Gorelick, S.M., 2005. Saline tracer visualized with three dimensional electrical resistivity tomography: field-scale spatial moment analysis, *Water Resour. Res.,* **41,** W05023, doi:10.1029/2004WR003460.

Singha, K., Pidlisecky, A., Day-Lewis, F.D. & Gooseff, M.N., 2008. Electrical characterization of non-Fickian transport in groundwater and hyporheic systems, *Water Resour. Res.,* **44,** W00D07, doi:10.1029/2008WR007048.

Skold M., Revil A., & Vaudelet P., 2011. The pH dependence of spectral induced polarization of silica sands: experiment and modeling, *Geophys. Res. Lett.,* **38,** L12304, doi:10.1029/2011GL047748.

Slater, L. & Lesmes, D., 2002. Electrical-hydraulic relationships observed for unconsolidated sediments, *Water Resour. Res.,* **38**(10), 1213, doi:10.1029/2001WR001075.

Sverjensky, D.A., 2005. Prediction of surface charge on oxydes in salt solutions: revisions for 1:1 (M^+L^-) electrolytes, *Geochim. Cosmochim. Acta,* **60,** 3773–3798.

Tarasov, A. & Titov, K., 2007. Relaxation time distribution from time domain induced polarization measurements, *Geophys. J. Int.,* **170,** 31–43.

Titov, K., Komarov, V., Tarasov, V. & Levitski, A., 2002. Theoretical and experimental study of time domain induced polarization in water-saturated sands, *J. appl. Geophys.,* **50,** 417–433.

Vaudelet, P., Revil, A., Schmutz, M., Franceschi, M., & Bégassat, P., 2011a. Induced polarization signature of the presence of copper in saturated sands, *Water Resour. Res.,* **47,** W02526, doi:10.1029/2010WR009310.

Vaudelet, P., Revil, A., Schmutz, M., Franceschi, M., & Bégassat, P., 2011b. Changes in induced polarization associated with the sorption of sodium, lead, and zinc on silica sands, *J. Coll. Interface Sci.,* **360,** 739–752.

Vinegar, H.J. & Waxman, M.H., 1984. Induced polarization of shaly sands, *Geophysics,* **49,** 1267–1287.

Wagner, K.W., 1914. Erklärung der dielektrischen Nachwirkungsvorgänge auf Grund Maxwellscher Vorstellungen, *Archiv. für Electrotechnik,* **2,** 371–387.

Wang, M. & Revil, A., 2010. Electrochemical charge of silica surface at high ionic strength in narrow channels, *J. Coll. Interface Sci.,* **343,** 381–386.

Watillon, A. & de Backer, R., 1970. Potentiel d'écoulement, courant d'écoulement et conductance de surface à l'interface eau-verre, *J. Electroanal. Chem. Interfacial Electrochem.,* **25,** 181–196.

Williams, K.H. *et al*., 2009. Geophysical monitoring of microbial activity during stimulated subsurface bioremediation, *J. Environ. Sci. Technol.,* **43**(17), 6717–6723, doi:10.1021/es900855.

Zimmermann, E., Kemna, A., Berwix, J., Glaas, W., Münch, H.M. & Huisman, J.A., 2008. A high-accuracy impedance spectrometer for measuring sediments with low polarizability, *Meas. Sci. Technol*., **19,** doi:10.1088/0957-0233/19/10/105603.

APPENDIX: SORPTION ISOTHERM

To solve the sorption isotherm, we use the two equilibrium relationships:

$$K_{(-)} = \frac{\Gamma^0_{\mathrm{SiO^-}} \left[\mathrm{H^+}\right]^0}{\Gamma^0_{\mathrm{SiOH}}}, \tag{A1}$$

$$K_{\mathrm{Na}} = \frac{\Gamma^0_{\mathrm{SiONa}} \left[\mathrm{H^+}\right]^0}{\Gamma^0_{\mathrm{SiOH}} \left[\mathrm{Na^+}\right]^0} \tag{A2}$$

and a continuity equation for the conservation of the surface species

$$\Gamma^0_{\mathrm{S}} = \Gamma^0_{\mathrm{SiONa}} + \Gamma^0_{\mathrm{SiOH}} + \Gamma^0_{\mathrm{SiO^-}}. \tag{A3}$$

We simplify the notations using $\mathrm{pH} = -\log_{10}\,[\mathrm{H^+}]$ and $[\mathrm{Na^+}]^0 = C_f$. Neglecting the effect of the surface potential on the activity of the protons in eq. (A1), the resolution of these three equations (A1)–(A3) is straightforward and yields

$$\Gamma^0_{\mathrm{SiONa}} = \Gamma^0_S \frac{K_{\mathrm{Na}} C_f}{K_{(-)} + 10^{-\mathrm{pH}} + K_{\mathrm{Na}} C_f}. \tag{A4}$$

Note that from eq. (A4) at high salinity, the Stern layer is saturated by sodium and $\Gamma^0_{\mathrm{SiONa}} \approx \Gamma^0_S$. The specific surface conductivity is the Stern layer is given by

$$\Sigma_S = e\beta_{\mathrm{Na}} \Gamma^0_{\mathrm{SiONa}}. \tag{A5}$$

Combining eqs (A4) and (A5) yields the equation obtained in the main text. Note that in this derivation, we have ignored the change in the pH close to the mineral surface.

For calcium, the sorption reaction is given by

$$> \mathrm{SiOH^0} + \mathrm{Ca^{2+}} \Leftrightarrow > \mathrm{SiO^-Ca^{2+}} + \mathrm{H^+}, \tag{A6}$$

and the continuity equation is given as

$$\Gamma^0_{\mathrm{S}} = \Gamma^0_{\mathrm{SiOCa}} + \Gamma^0_{\mathrm{SiOH}} + \Gamma^0_{\mathrm{SiO^-}}. \tag{A7}$$

Therefore, following the same steps (A1)–(A5), we get

$$\Gamma^0_{\mathrm{SiOCa}} = \Gamma^0_S \frac{K_{\mathrm{Ca}} C_f}{K_{(-)} + 10^{-\mathrm{pH}} + K_{\mathrm{Ca}} C_f}, \tag{A8}$$

and the specific surface conductivity is given by $\Sigma_S = 2e\beta_{\mathrm{Ca}} \Gamma^0_{\mathrm{SiOCa}}$.